# Synthesis and Characterization of New Hybrid Organic-Inorganic Metal Halides [(CH<sub>3</sub>)<sub>3</sub>SO]M<sub>2</sub>I<sub>3</sub> (M = Cu, Ag)

Tamanna Pinky<sup>a</sup>, Dilruba A. Popy<sup>a</sup>, Zheng Zhang<sup>b</sup>, Jie Jiang<sup>c</sup>, Ruth Pachter<sup>c</sup>, Bayram Saparov<sup>a</sup>\*

<sup>a</sup>Department of Chemistry & Biochemistry, University of Oklahoma, Norman, OK 73019

<sup>b</sup>Department of Chemistry, Tulane University, New Orleans, LA 70118

<sup>c</sup> Air Force Research Laboratory, Materials and Manufacturing Directorate, Wright
Patterson Air Force Base, Ohio 45433

\*Author to whom correspondence should be addressed: <a href="mailto:saparov@ou.edu">saparov@ou.edu</a>

**Abstract:** Recently, all-inorganic copper(I) metal halides have emerged as promising optical materials due to their high light emission efficiencies. This work details the crystal structure of the two hybrid organic-inorganic metal halides [(CH<sub>3</sub>)<sub>3</sub>SO]M<sub>2</sub>I<sub>3</sub> (M = Cu, Ag) and their alloyed derivatives [(CH<sub>3</sub>)<sub>3</sub>SO]Cu<sub>2-x</sub>Ag<sub>x</sub>I<sub>3</sub> (x = 0.2; 1.25), which were obtained by incorporating trimethylsulfoxonium organic cation (CH<sub>3</sub>)<sub>3</sub>SO<sup>+</sup> in place of Cs<sup>+</sup> in the yellow-emitting all-inorganic CsCu<sub>2</sub>I<sub>3</sub>. These compounds are isostructural and centrosymmetric with the space group *Pnma*, featuring 1D edge-sharing [M<sub>2</sub>I<sub>3</sub>]<sup>-</sup> anionic double chains separated by rows of (CH<sub>3</sub>)<sub>3</sub>SO<sup>+</sup> cations. Based on the density functional theory (DFT) calculations, the highest occupied molecular orbitals (HOMOs) of [(CH<sub>3</sub>)<sub>3</sub>SO]M<sub>2</sub>I<sub>3</sub> (M = Cu, Ag) are dominated by the Cu or Ag *d* and I *p* orbitals, while the lowest unoccupied molecular orbitals (LUMOs) are Cu or Ag *s* and I *p* orbitals. [(CH<sub>3</sub>)<sub>3</sub>SO]Cu<sub>2</sub>I<sub>3</sub> single crystals exhibit a semiconductor resistivity of 9.94×10<sup>9</sup> Ω·cm. Furthermore, a prototype [(CH<sub>3</sub>)<sub>3</sub>SO]Cu<sub>2</sub>I<sub>3</sub> single crystal-based X-ray detector with a detection sensitivity of 200.54 uCGy<sup>-1</sup>cm<sup>-2</sup> (at electrical field E=41.67 V/mm) was fabricated, indicating the potential use of [(CH<sub>3</sub>)<sub>3</sub>SO]Cu<sub>2</sub>I<sub>3</sub> for radiation detection applications.

### 1. Introduction

In recent years, copper-based metal halides have received sustained attention as nontoxic alternatives for lead halide perovskites.<sup>1</sup> These materials are based on the inexpensive element copper and can be synthesized via both low-temperature solution processing and high-temperature synthesis, making them very good candidates for a variety of applications, including solid-state lighting, temperature and radiation sensing, and anti-counterfeiting.<sup>2-5</sup> To date, most attention has been devoted to several all-inorganic Cu(I) halide families including CsCu<sub>2</sub>X<sub>3</sub> (X = CI, Br, I), A<sub>2</sub>CuX<sub>3</sub> (A= K, Rb; X = CI, Br), Cs<sub>3</sub>Cu<sub>2</sub>X<sub>5</sub> (X = Br, I), and Cs<sub>5</sub>Cu<sub>3</sub>Cl<sub>6</sub>I<sub>2</sub>.<sup>2, 3, 5-8</sup> Each family adopts a unique low-dimensional crystal structure that facilitates strong charge localization and formation of room-temperature self-trapped excitonic (STE) states resulting in up to unity quantum yield light emission efficiency.<sup>2, 3, 5, 6</sup>

Notably, the CsCu<sub>2</sub>X<sub>3</sub> ("123") family is reported to have the best overall air, thermal, and photostability compared to the other alkali Cu(I) halides. 6, 7, 9, 10 In contrast to the blueemitting Cs<sub>3</sub>Cu<sub>2</sub>X<sub>5</sub> and A<sub>2</sub>CuX<sub>3</sub>, CsCu<sub>2</sub>X<sub>3</sub> (X = Cl, Br, I) also have a wider range of emission wavelengths from green to yellow, allowing for both the study of compositionstructure-property trends and the property tuning for targeted optical applications.<sup>6, 7, 10, 11</sup> CsCu<sub>2</sub>X<sub>3</sub> structures feature 1D [Cu<sub>2</sub>X<sub>3</sub>] anionic chains formed by edge-sharing Cu<sup>1</sup>X<sub>4</sub> tetrahedra.<sup>2, 6, 7</sup> Interestingly, the "123" family members demonstrate the lowest photoluminescence efficiencies among all-inorganic Cu(I) halides, which could be explained by considering the structural differences among all-inorganic Cu(I) halides including smaller interchain distances in 1D CsCu<sub>2</sub>X<sub>3</sub>.<sup>2</sup> The latter could be an important parameter, as CsCu<sub>2</sub>X<sub>3</sub> exhibit greater charge delocalization compared to the other known low-dimensional alkali Cu(I) halides, which in turn could explain the lower light emission efficiencies observed in this family.<sup>2, 7, 10</sup> To check the validity of the proposed explanations, additional studies focused on increasing inter-chain distances and greater charge localization in the "123" family are needed. This can be achieved by replacing Cs+ cations in CsCu<sub>2</sub>X<sub>3</sub> with organic cations, which has been a popular strategy for controlling the distances between polyanionic units in hybrid organic-inorganic metal halides. 12-17

This study focuses on understanding the fundamental structure-property relationships in the "123" family. In this family, CsCu<sub>2</sub>I<sub>3</sub> has attracted most attention due to its promising performance in a number of applications including photodetectors, radiation detector, light-emitting diodes (LEDs), and X-ray imaging.<sup>1, 2, 7, 10, 18-26</sup> Although CsCu<sub>2</sub>I<sub>3</sub> has the lowest reported photoluminescence quantum yield (PLQY) value of 3.23% among the alkali Cu(I) halides,<sup>7</sup> its inclusion as a dopant in organic host materials can significantly boost the PLQY and enable its use in efficient LEDs.<sup>25</sup> Notwithstanding

the engineering approach to improve the optoelectronic properties of this material, question remains if crystal-chemical modifications could also improve relevant properties of CsCu<sub>2</sub>I<sub>3</sub> for practical applications including light emission efficiency. The chemical approaches would also be valuable for fundamental understanding of composition-structure-property relationships in this materials family. Only a single hybrid organic-inorganic "123" compound, [Me-MePy]Cu<sub>2</sub>I<sub>3</sub>, has been reported to date; it crystallizes in the *Pnma* space group and contains 1D [Cu<sub>2</sub>I<sub>3</sub>]<sup>-</sup> chains that are separated by [Me-MePy]<sup>+</sup> cations.<sup>27</sup> However, the incorporation of [Me-MePy]<sup>+</sup> cations in place of Cs<sup>+</sup> in CsCu<sub>2</sub>I<sub>3</sub> only slightly increases the interchain distances and the reported photoluminescence efficiency of 3.85% is comparable to that of CsCu<sub>2</sub>I<sub>3</sub>.<sup>27</sup>

Another possible strategy to boost the PLQY of CsCu<sub>2</sub>I<sub>3</sub> (heretofore untested), is through a gradual substitution of Cu<sup>+</sup> with Ag<sup>+</sup>. This follows the idea that Cu<sup>+</sup> cations act as optical centers in alkali Cu(I) halides as the top of the valence and bottom of the conduction bands are dominated by Cu-3*d* and Cu-4*s* orbitals, respectively. Therefore, gradual incorporation of Ag<sup>+</sup> instead of Cu<sup>+</sup> could modify optical properties and boost PLQY of the "123" Cu(I) halides. In addition, the Ag<sup>+</sup> inclusion could also improve the stability of Cu(I) halides as the oxidation of Cu<sup>+</sup> to Cu<sup>2+</sup> is a known cause for the poor stability of some of the alkali Cu(I) halides. However, to date, there are no reports of solid solution behavior for any Cu(I) halide families. Instead, there have been reports of analogous Ag(I) halides such as CsAg<sub>2</sub>I<sub>3</sub>, <sup>28-30</sup> Rb<sub>2</sub>AgX<sub>3</sub>, (NH<sub>4</sub>)<sub>2</sub>AgX<sub>3</sub> (X = CI, Br, I), etc.<sup>31</sup>, <sup>32</sup> Although these Ag(I) halides are reportedly more stable compared to their Cu(I) analogs, their PL emission efficiencies are typically lower.<sup>2</sup>

In this study, we report preparation, crystal structures, and optical properties of two new 1D hybrid copper(I) and silver(I) halides, [(CH<sub>3</sub>)<sub>3</sub>SO]Cu<sub>2</sub>I<sub>3</sub>, [(CH<sub>3</sub>)<sub>3</sub>SO]Ag<sub>2</sub>I<sub>3</sub>, and their alloyed derivatives [(CH<sub>3</sub>)<sub>3</sub>SO]Cu<sub>2-x</sub>Ag<sub>x</sub>I<sub>3</sub> (x = 0.2; 1.25). These compounds are members of the "123" family obtained by incorporating trimethylsulfoxonium organic cation ((CH<sub>3</sub>)<sub>3</sub>SO<sup>+</sup>) in place of Cs<sup>+</sup> in the yellow-emitting CsCu<sub>2</sub>I<sub>3</sub>. The incorporation of the larger organic cation increases the interchain distances, however, only a minor expansion is achieved and the halide anions are closely packed in [(CH<sub>3</sub>)<sub>3</sub>SO]Cu<sub>2-x</sub>Ag<sub>x</sub>I<sub>3</sub>. Consequently, the reported materials exhibit weak photoluminescence (PL) emission properties. Here, the discussions of crystal structures and optical properties of the obtained compounds are supported by density functional theory (DFT) calculations.

### 2. Experimental section

#### 2.1. Materials

Copper(I) iodide (>99%, Sigma-Aldrich), silver iodide (99.999%, Alfa Aesar), trimethylsulfoxonium iodide (98%, Sigma-Aldrich), N,N-dimethylformamide (DMF) (99%, Fisher), diethyl ether anhydrous (Fisher), hypophosphorous acid (H<sub>3</sub>PO<sub>2</sub>) (50%, Sigma-Aldrich) were used as purchased without further purification. Reactions containing silver reagents were carried out in glass reaction vials wrapped in aluminum foil to prevent photodegradation. All synthesis experiments were carried out in ambient air inside a fume hood, unless specified otherwise.

# 2.2. [(CH<sub>3</sub>)<sub>3</sub>SO]Cu<sub>2</sub>l<sub>3</sub> single crystal growth via vapor-diffusion

[(CH<sub>3</sub>)<sub>3</sub>SO]Cu<sub>2</sub>I<sub>3</sub> single crystals were synthesized by mixing 1 mmol of (CH<sub>3</sub>)<sub>3</sub>SOI and 2 mmol of CuI in a glass vial, followed by the addition of 3 mL of DMF and 0.1 mL of H<sub>3</sub>PO<sub>2</sub> with stirring at room temperature to form a clear solution. Next, the precursor solution was transferred to a sealed container containing 4 mL of diethyl ether. Overnight, diethyl ether was introduced into the precursor solution by vapor diffusion at room temperature. The controlled vapor-diffusion process allowed the formation of colorless block crystals with the dimensions of approximately 0.3 cm. These crystals were carefully collected from the solution, washed with diethyl ether to remove any impurities, and dried at room temperature. The crystals were stored inside the nitrogen-filled glove box for subsequent property measurements.

## 2.3. [(CH<sub>3</sub>)<sub>3</sub>SO]Ag<sub>2</sub>I<sub>3</sub> single crystal growth via vapor-diffusion

[(CH<sub>3</sub>)<sub>3</sub>SO]Ag<sub>2</sub>I<sub>3</sub> single crystals were synthesized by mixing 1 mmol of (CH<sub>3</sub>)<sub>3</sub>SOI and 2 mmol of AgI in a 20 mL glass vial, followed by the addition of 5 mL of DMF. The vial was then capped and heated at 60°C until complete dissolution of all reactants occurred. Subsequently, the clear solution was then cooled down to room temperature and placed into another vial containing 6 mL of diethyl ether solution, which served as an anti-solvent. The colorless needle shape crystals of [(CH<sub>3</sub>)<sub>3</sub>SO]Ag<sub>2</sub>I<sub>3</sub> were carefully collected after one day and stored in a nitrogen-filled glovebox for property characterization.

# 2.4. [(CH<sub>3</sub>)<sub>3</sub>SO]Cu<sub>2-x</sub>Ag<sub>x</sub>I<sub>3</sub> (nominal x = 0.2, 0.4, 1, 1.4) single crystal growth via vapor-diffusion

[(CH<sub>3</sub>)<sub>3</sub>SO]Cu<sub>2-x</sub>Ag<sub>x</sub>I<sub>3</sub> compounds were prepared by mixing stoichiometric amounts of (CH<sub>3</sub>)<sub>3</sub>SOI and MX (M = Cu, Ag) in 4 mL of DMF, along with 0.1 mL of H<sub>3</sub>PO<sub>2</sub> at room temperature. The resultant reaction mixture was then subjected to counter vapor diffusion with diethyl ether in a closed vial. The best-quality crystals were obtained from the nominal x loadings of 0.2 and 1, with only small compositional deviations. Detailing in the results and discussion section.

### 2.6. Powder X-ray diffraction (PXRD) measurements

Powder X-ray diffraction (PXRD) measurements were conducted at room temperature on a Rigaku MiniFlex600 system that utilizes a Ni-filtered Cu K $\alpha$  radiation source. All the measurements were carried out by grinding single crystals into fine powders; the PXRD scans covered the 3 – 90° (20) range, with a step size of 0.02°. Data analysis was performed using the PDXL2 software package and obtained XRD patterns were fitted using the decomposition method. Powder samples were exposed to ambient air (20°C and 30% relative humidity) for three months and their PXRD patterns were recorded periodically during this time to assess their air-stability.

## 2.7. Single crystal X-ray diffraction (SCXRD) measurements

A Bruker D8 Quest diffractometer with a Kappa-geometry configuration was used for SCXRD measurements. The diffractometer was equipped with an Incoatec Iµs microfocus Mo Kα X-ray source, and data acquisition was performed using a Photon II area detector. Absorption corrections were applied by the semiempirical method, which relies on equivalent reflections. Crystal structures were determined using intrinsic phasing methods incorporated into the APEX3 v2015.5-2 program. Details of the data collection and crystallographic parameters can be found in Tables S1 and S5. Atomic coordinates, equivalent isotropic displacement parameters, as well as selected interatomic distances and bond angles, can be found in the Supporting information (SI). The Crystallographic Information Files (CIFs) can be found in the Cambridge Crystallographic Data Centre (CCDC) database (deposition numbers 2303067-2303070).

# 2.8. Differential scanning calorimetry (DSC) and thermogravimetric analysis (TGA) measurements

DSC and TGA measurements were performed using a TA Instruments SDT650 unit. The experiments utilized 90  $\mu$ L alumina crucibles, and each sample weighed ~10 mg. The measurements were conducted under a nitrogen flow rate of 100 mL/min, in the temperature range of 30 - 475 °C with a heating rate of 10 °C/min. The DSC onset temperatures were determined using TA Instrument's TRIOS software analysis package.

#### 2.9. Photoluminescence measurements

HORIBA Jobin Yvon Fluorolog-3 spectrofluorometer equipped with a Xenon lamp source and Quanta-Φ integrating sphere used to perform room-temperature photoluminescence excitation (PLE) and emission (PL) measurements on single crystal samples of the respective compounds mentioned in this work. Data acquisition was accomplished using the two-curve method in a varied wavelength range of 250 to 750 nm.

### 2.10. Diffuse reflectance measurements

To study the optical bandgap energy of the compounds mentioned, we used a PerkinElmer Lambda 750 UV-vis-NIR spectrometer equipped with a 100 mm Spectralon InGaAs Integrating Sphere. The spectrometer covered a wavelength range of 250-1100 nm. Diffuse reflectance data were converted into pseudo-absorption spectra using the Kubelka-Munk function. The function is represented as  $F(R) = \frac{\alpha}{S} = \frac{(1-R)^2}{2R}$ , where  $\alpha$  denotes the absorption coefficient, S is the scattering coefficient, and R is the reflectance.

# 2.11. Density Functional Theory (DFT) Calculations

DFT calculations were carried out with the Vienna ab initio simulation package VASP 5.4.<sup>34, 35</sup> The Kohn-Sham equations are solved using a plane wave basis set with an energy cutoff of 500 eV, and the projector augmented-wave (PAW) potential was applied.<sup>35</sup> A 8×5×3 *k*-point sampling was used for unit cell. The crystal structure was optimized using the PBE functional,<sup>36</sup> including the zero damping D3 correction of Grimme,<sup>37</sup> as inclusion of London dispersion for treating halide perovskites was emphasized,<sup>38</sup> and previously applied.<sup>39</sup> Geometries were fully relaxed regarding lattice parameters and interatomic distances until forces were less than 0.01 eV/Å.

# 2.12. Scanning Electron Microscopy (SEM) and Energy Dispersive X-ray Spectroscopy (EDS)

A conventional tungsten filament SEM with secondary electron imaging and EDS microscopy (FEI Quanta SEM) system was used for crystal morphology imaging, elemental mapping, and compositional analysis. At least three crystals from each reaction system were selected under an optical microscope and placed on top of a sample holder covered with carbon tape. Compositional analysis was performed on at least 3 separate regions of each crystal.

### 2.13. Electrical measurements and X-ray response tests

For electrical measurements and evaluating the X-ray response characteristics, a prototype X-ray detector was fabricated by brushing high-quality silver paste (purchased from Ted Pella, Inc.) onto the two opposite sides of a single crystal of [(CH<sub>3</sub>)<sub>3</sub>SO]Cu<sub>2</sub>I<sub>3</sub>. Keithley 6487 pico-ammeter was used to conduct current-voltage (I-V) and space-charge-limited-current (SCLC) measurements. For X-ray response test, the fabricated prototype detector was exposed to soft X-rays of 8 keV, which were generated by a Rigaku MicroMax 007HF microfocus X-ray generator equipped with a Cu target. X-ray radiation dose rate was carefully calibrated using a commercial dosimeter.

### 3. Results and Discussion

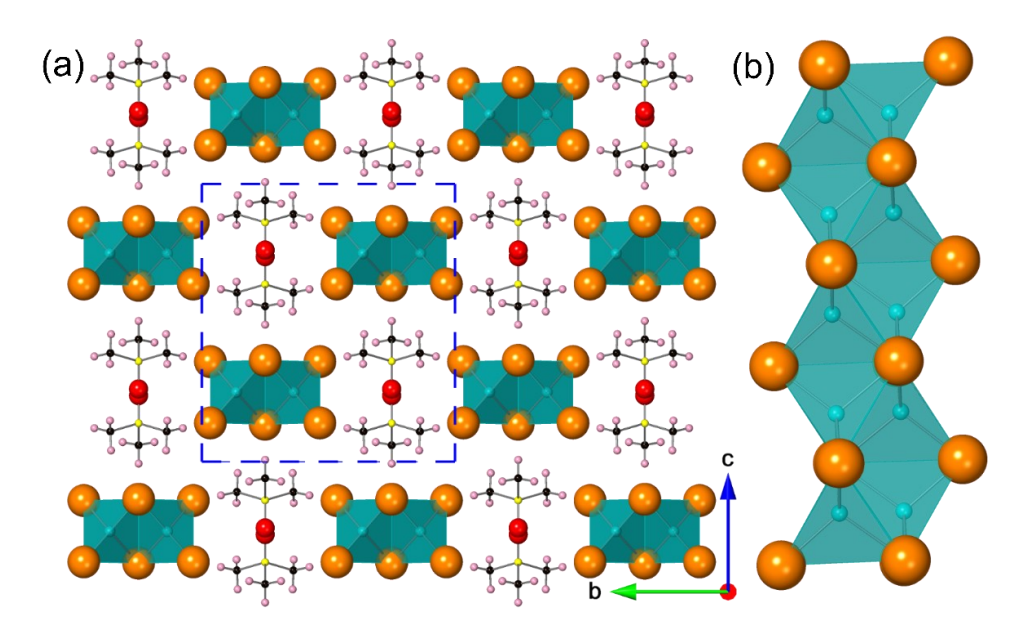


**Figure 1.** (a) Crystal structure of  $[(CH_3)_3SO]M_2I_3$  (M = Cu, Ag) projected down the *a*-axis. Cyan, orange, yellow, red, pink, and black spheres represent metal (copper, silver), iodine, sulfur, oxygen, hydrogen, and carbon atoms, respectively. (b) A close-up view of the polyanionic  $[M_2I_3]^-$  chain showing the edge-sharing connectivity of MI<sub>4</sub> tetrahedra.

Colorless single crystals of [(CH<sub>3</sub>)<sub>3</sub>SO]Cu<sub>2</sub>I<sub>3</sub>, and [(CH<sub>3</sub>)<sub>3</sub>SO]Ag<sub>2</sub>I<sub>3</sub>, were grown from the corresponding organic salt and metal halides by the anti-solvent vapor diffusion method. The detailed synthesis techniques are described in the experimental section. The obtained transparent single crystals of [(CH<sub>3</sub>)<sub>3</sub>SO]Cu<sub>2</sub>I<sub>3</sub>, and [(CH<sub>3</sub>)<sub>3</sub>SO]Ag<sub>2</sub>I<sub>3</sub> can be up to 0.3-centimeter long and are colorless, indicating that these compounds may have wide optical band gaps and minimal visible region absorptions (Figure S1).

Tables S1–S4 summarize the results of SCXRD experiments performed at 100 K. [(CH<sub>3</sub>)<sub>3</sub>SO]Cu<sub>2</sub>l<sub>3</sub> and [(CH<sub>3</sub>)<sub>3</sub>SO]Ag<sub>2</sub>l<sub>3</sub> are isostructural and crystallize in the centrosymmetric orthorhombic space group *Pnma*. Their structures consist of one-dimensional (1D) [M<sub>2</sub>l<sub>3</sub>]<sup>-</sup> anionic double chains separated by (CH<sub>3</sub>)<sub>3</sub>SO<sup>+</sup> cations. The [M<sub>2</sub>l<sub>3</sub>]<sup>-</sup> ribbons are formed by an edge-sharing connectivity of the respective metal halide tetrahedra in one crystallographic direction (the *a*-axis). Thus, [(CH<sub>3</sub>)<sub>3</sub>SO]Cu<sub>2</sub>l<sub>3</sub> and [(CH<sub>3</sub>)<sub>3</sub>SO]Ag<sub>2</sub>l<sub>3</sub> belong to the family of "123" compounds. In fact, [(CH<sub>3</sub>)<sub>3</sub>SO]Cu<sub>2</sub>l<sub>3</sub> is a substitutional hybrid analog of the yellow emitter CsCu<sub>2</sub>l<sub>3</sub>.<sup>7</sup> The substitution of Cs<sup>+</sup> with (CH<sub>3</sub>)<sub>3</sub>SO<sup>+</sup> cations in CsCu<sub>2</sub>l<sub>3</sub>, however, results in the change of the structural symmetry as CsCu<sub>2</sub>l<sub>3</sub> is known to crystallize in the orthorhombic space group of *Cmcm*. In CsCu<sub>2</sub>l<sub>3</sub>, the Cu-I distances in [Cu<sub>2</sub>l<sub>3</sub>]<sup>-</sup> range from 2.604(2) Å to 2.703(4) Å, and the I-Cu-I angles range from 107.10(2)° to 114.24(4)°. In comparison, the individual Cul<sub>4</sub> tetrahedra in

[(CH<sub>3</sub>)<sub>3</sub>SO]Cu<sub>2</sub>I<sub>3</sub> are slightly more distorted with Cu-I bond distances ranging from 2.6065(5) Å to 2.7230(5) Å, and the I-Cu-I bond angles varying from 103.244(18)° to 119.729(19)° (Table S4 and Figure S2). Another similar edge-sharing 1D [Cu<sub>2</sub>I<sub>3</sub>]<sup>-</sup> chain structure observed in [Me-MePy]Cu<sub>2</sub>I<sub>3</sub> features Cu-I bond distances in the range of 2.6084(6) – 2.7305(6) Å, almost identical to that of [(CH<sub>3</sub>)<sub>3</sub>SO]Cu<sub>2</sub>I<sub>3</sub>.<sup>27</sup> In CsCu<sub>2</sub>I<sub>3</sub> the shortest interchain distance between the neighboring [Cu<sub>2</sub>I<sub>3</sub>]<sup>-</sup> chains is *d*(I-I) = 4.126 Å. This distance increase slightly to 4.328 Å for [Me-MePy]Cu<sub>2</sub>I<sub>3</sub> and further to 4.447 Å for compound [(CH<sub>3</sub>)<sub>3</sub>SO]Cu<sub>2</sub>I<sub>3</sub>, slightly higher than twice of the iodide anion radius (4.4 Å). Indeed, this observation supports the success of our cation replacement approach for increasing the interchain distance. However, even in the hybrid analogs of CsCu<sub>2</sub>I<sub>3</sub>, the interchain distances remain quite short and the halide anions are closely packed, which is likely to result in unusually dispersive bands around the Fermi level for a low-dimensional Cu(I) halide structure (see below).<sup>2</sup>

Attempts to synthesize the silver (Ag) counterpart of [(CH<sub>3</sub>)<sub>3</sub>SO]Cu<sub>2</sub>I<sub>3</sub> result in the formation of [(CH<sub>3</sub>)<sub>3</sub>SO]Ag<sub>2</sub>I<sub>3</sub>, which crystallizes in the same space group *Pnma* as [(CH<sub>3</sub>)<sub>3</sub>SO]Cu<sub>2</sub>I<sub>3</sub> and is isostructural to it. Its all-inorganic counterpart CsAg<sub>2</sub>I<sub>3</sub> has reportedly a similar 1D structure but a different space group of *Pbnm*.<sup>28-30, 33</sup> The observed distortions in the [Ag<sub>2</sub>I<sub>3</sub>]<sup>-</sup> chains in [(CH<sub>3</sub>)<sub>3</sub>SO]Ag<sub>2</sub>I<sub>3</sub> are comparable to that of [(CH<sub>3</sub>)<sub>3</sub>SO]Cu<sub>2</sub>I<sub>3</sub>; [(CH<sub>3</sub>)<sub>3</sub>SO]Ag<sub>2</sub>I<sub>3</sub> features Ag-I bond lengths varying from 2.7857(5) Å to 2.9345(5) Å and the I-Ag-I angles range from 103.301(17)° to 120.400(18)°. To date, there are only a few examples of hybrid silver halides. In 1980s, Kildea et al. reported an isostructural hybrid compound (Me<sub>4</sub>N)Ag<sub>2</sub>I<sub>3</sub>; the Ag-I bond lengths vary from 2.780(2) Å to 2.966(2) Å and I-Ag-I angles range from 99.84(5)° to 119.86(7)° in (Me<sub>4</sub>N)Ag<sub>2</sub>I<sub>3</sub>.<sup>40, 41</sup>

Since [(CH<sub>3</sub>)<sub>3</sub>SO]Cu<sub>2</sub>I<sub>3</sub> and [(CH<sub>3</sub>)<sub>3</sub>SO]Ag<sub>2</sub>I<sub>3</sub> are isostructural, we performed reactions to prepare alloyed [(CH<sub>3</sub>)<sub>3</sub>SO]Cu<sub>2-x</sub>Ag<sub>x</sub>I<sub>3</sub> (x = 0.2, 0.4, 1, 1.4) compositions. Our bulk synthesis experiments suggest (Figure S4) that Vegard's law is not strictly followed in this system. Therefore, for further structural and physical property characterizations, we worked on single crystalline samples of alloyed compositions. Tables S5–S7 summarize the results of SCXRD experiments performed at 100 K for two alloyed compositions, [(CH<sub>3</sub>)<sub>3</sub>SO]Cu<sub>1.80(1</sub>)Ag<sub>0.20(1</sub>)I<sub>3</sub> and [(CH<sub>3</sub>)<sub>3</sub>SO]Cu<sub>0.75(1</sub>)Ag<sub>1.25(1</sub>)I<sub>3</sub>. We observed a slight deviation from the nominal value for the equimolar Cu(I)/Ag(I) iodide loading ratio, which produced [(CH<sub>3</sub>)<sub>3</sub>SO]Cu<sub>0.75(1</sub>)Ag<sub>1.25(1</sub>)I<sub>3</sub>. [(CH<sub>3</sub>)<sub>3</sub>SO]Cu<sub>1.80(1</sub>)Ag<sub>0.20(1</sub>)I<sub>3</sub> and [(CH<sub>3</sub>)<sub>3</sub>SO]Cu<sub>0.75(1</sub>)Ag<sub>1.25(1</sub>)I<sub>3</sub> are isostructural to the parent end members [(CH<sub>3</sub>)<sub>3</sub>SO]Cu<sub>2</sub>I<sub>3</sub> and [(CH<sub>3</sub>)<sub>3</sub>SO]Ag<sub>2</sub>I<sub>3</sub> which crystallize in the *Pnma* space group. To further confirm the obtained chemical compositions and homogeneous distribution of Cu and Ag in individual single crystals, SEM-EDS measurements were performed (Figure S7-S8, and Table S8).

The results obtained from SEM-EDS are in good agreement with the data obtained from SCXRD experiments.

Since the composition of [(CH<sub>3</sub>)<sub>3</sub>SO]Cu<sub>1.80(1)</sub>Ag<sub>0.20(1)</sub>I<sub>3</sub> is closer to that of [(CH<sub>3</sub>)<sub>3</sub>SO]Cu<sub>2</sub>I<sub>3</sub>, the M-I bond distances ranging from 2.5993(15) Å to 2.7768(14) Å and the I-M-I angles ranging from 103.21(5)° to 121.87(6)° are close to that observed in [(CH<sub>3</sub>)<sub>3</sub>SO]Cu<sub>2</sub>I<sub>3</sub> (Figure S2). Similarly, the composition of [(CH<sub>3</sub>)<sub>3</sub>SO]Cu<sub>0.75(1)</sub>Aq<sub>1.25(1)</sub>I<sub>3</sub> is closer to that of [(CH<sub>3</sub>)<sub>3</sub>SO]Ag<sub>2</sub>I<sub>3</sub>, and the observed M-I bond distances (2.624(5) to 3.004(5) Å) and I-M-I angles (104.73(5) to 118.33(9)°) in [(CH<sub>3</sub>)<sub>3</sub>SO]Cu<sub>0.75(1)</sub>Ag<sub>1.25(1)</sub>I<sub>3</sub> are also closer to that of the Ag(I) halide parent [(CH<sub>3</sub>)<sub>3</sub>SO]Ag<sub>2</sub>I<sub>3</sub>. Unsurprisingly, the variations in bond distances and angles larger are for the alloyed  $[(CH_3)_3SO]Cu_{1.80(1)}Ag_{0.20(1)}I_3$  and  $[(CH_3)_3SO]Cu_{0.75(1)}Ag_{1.25(1)}I_3$  as compared to the parents. Note that the lattice parameters obtained from SCXRD data for the mixed compositions also do not follow a strict linear trend as a function of composition as is typically expected (i.e., Vegard's law, Figure S5). This is not unusual for the lowdimensional metal halides of the "123" family, 7 and even more so, for the low dimensional hybrid metal halides as the strict dense packing is not always followed due to the organic molecular components in the structure. 42-44 In the present case, we observe that while the parameter a increases significantly with increasing Ag content (~5.3% expansion), b and c remain almost unchanged with only slight increases of ~0.67% and 0.23%, respectively. This is because the  $[M_2I_3]^-$  chains extend along the a-axis in the structure, and therefore, the substitution of Cu<sup>+</sup> with larger Ag<sup>+</sup> has a noticeable impact on the parameter a. In contrast, the b- and c-axes correspond to the interchain directions to which metal substitution has only a minimal impact.

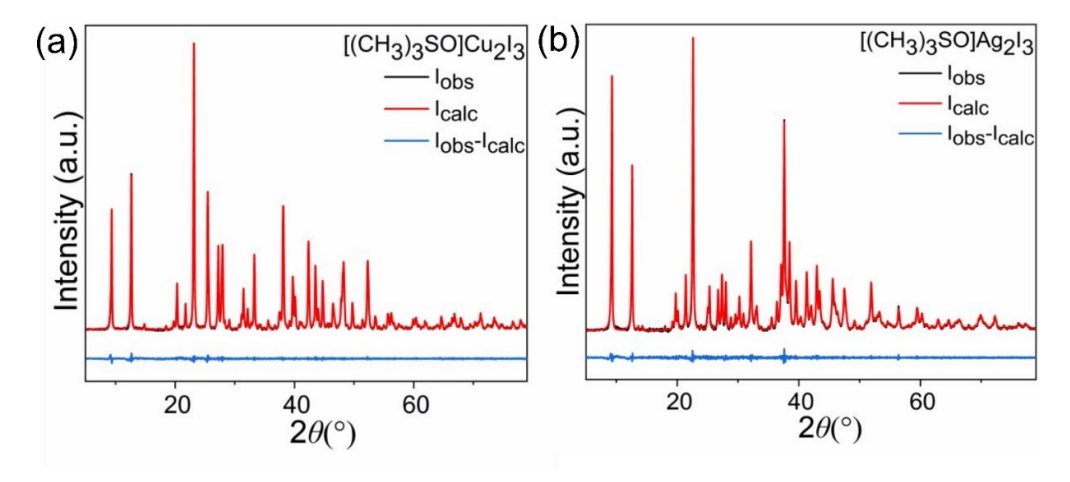


**Figure 2.** Room-temperature PXRD patterns (in black) fitted using the Pawley method (in red) for (a) [(CH<sub>3</sub>)<sub>3</sub>SO]Cu<sub>2</sub>I<sub>3</sub>, and (b) [(CH<sub>3</sub>)<sub>3</sub>SO]Ag<sub>2</sub>I<sub>3</sub>. Differences between the measured and calculated patterns are shown in blue.

To assess the phase purity and crystallinity of the as-synthesized products, powder X-ray Diffraction (PXRD) analysis was carried out. PXRD measurements suggest that there are no impurities in the samples (Figure 2). To evaluate the stability of the samples under ambient air, periodic PXRD measurements were conducted over a time span of 3 months. Throughout the monitoring period, none of the samples exhibited any signs of degradation or decomposition (Figure S3). This is in contrast to the poor air stability of some of the well-known all-inorganic Cu(I) halide light emitters. <sup>16,17,19</sup>

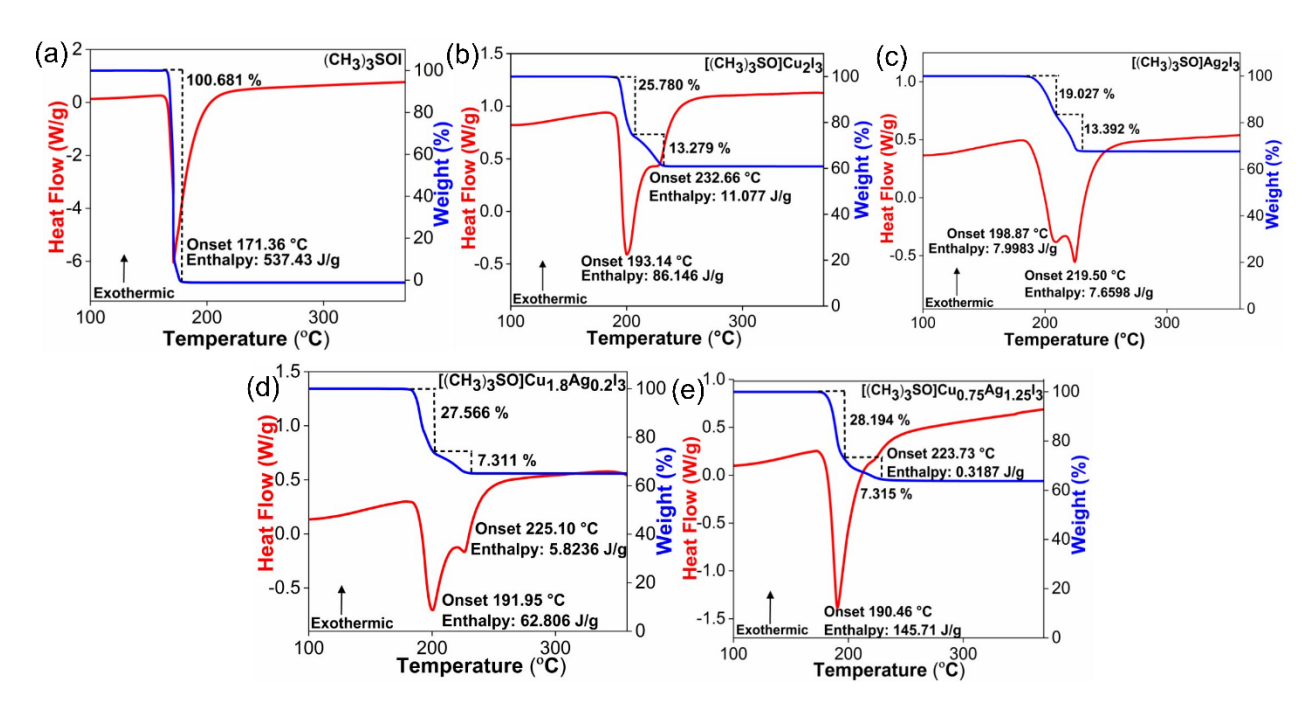


**Figure 3.** Thermogravimetric Analysis (TGA, in blue) and Differential Scanning Calorimetry (DSC, in red) plots for (a) (CH<sub>3</sub>)<sub>3</sub>SOI, (b) [(CH<sub>3</sub>)<sub>3</sub>SO]Cu<sub>2</sub>I<sub>3</sub>, (c) [(CH<sub>3</sub>)<sub>3</sub>SO]Ag<sub>2</sub>I<sub>3</sub>, (d) [(CH<sub>3</sub>)<sub>3</sub>SO]Cu<sub>1.80(1)</sub>Ag<sub>0.20(1)</sub>I<sub>3</sub>, and (e) [(CH<sub>3</sub>)<sub>3</sub>SO]Cu<sub>0.75(1)</sub>Ag<sub>1.25(1)</sub>I<sub>3</sub>.

Simultaneous DSC and TGA measurements were also performed to evaluate the thermal properties of the title compounds (Figure 3). The degradation of the precursor organic salt (CH<sub>3</sub>)<sub>3</sub>SOI occurs at 171 °C. In contrast, the thermal stabilities of title compounds are improved, with the onset thermal decomposition temperatures above 190°C. In each case, two thermal events can be observed both in DSC and TGA curves. The onset temperatures for the first thermal decomposition of [(CH<sub>3</sub>)<sub>3</sub>SO]Cu<sub>2</sub>I<sub>3</sub>, [(CH<sub>3</sub>)<sub>3</sub>SO]Cu<sub>1.80(1)</sub>Ag<sub>0.20(1)</sub>I<sub>3</sub>, and [(CH<sub>3</sub>)<sub>3</sub>SO]Cu<sub>0.75(1)</sub>Ag<sub>1.25(1)</sub>I<sub>3</sub> were recorded as 193.14 °C, 198.87 °C, 191.95 °C, and 190.46 °C, respectively. Upon further heating, another endothermic event occurs, corresponding to the second decomposition step at 232.66 °C, 219.50 °C, 225.10 °C, and 223.73 °C, respectively. However, it is important to note that these onset points do not correspond to the melting transition

accompanied by sample evaporation as the melting transition was checked for each compound within the temperature range of 40 °C to 320 °C; no melting transition was observed for all compounds within this window. The observed total weight loss percentages of [(CH<sub>3</sub>)<sub>3</sub>SO]Cu<sub>2</sub>I<sub>3</sub>, [(CH<sub>3</sub>)<sub>3</sub>SO]Ag<sub>2</sub>I<sub>3</sub>, [(CH<sub>3</sub>)<sub>3</sub>SO]Cu<sub>1.80(1)</sub>Ag<sub>0.20(1)</sub>I<sub>3</sub>, and [(CH<sub>3</sub>)<sub>3</sub>SO]Cu<sub>0.75(1)</sub>Ag<sub>1.25(1)</sub>I<sub>3</sub> (39.05%, 32.42%, 34.88%, and 35.50%) approximately match the weight of (CH<sub>3</sub>)<sub>3</sub>SOI in each compound (36.62%, 31.91%, 36.08%, and 33.52%, respectively). This suggests that the decomposition is likely caused by the thermal degradation and evaporation of the organic structural component.

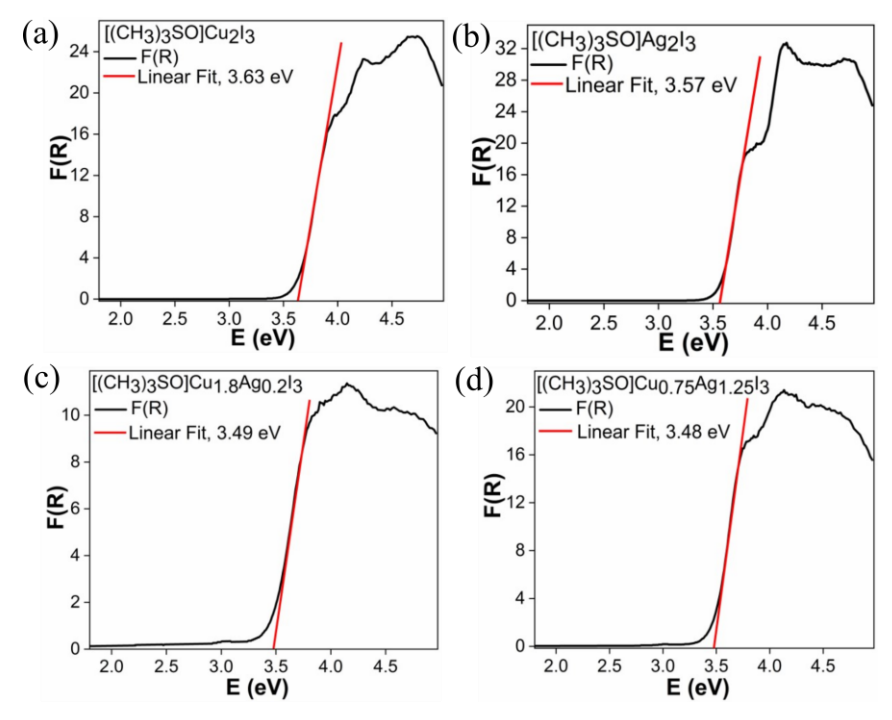


**Figure 4.** Optical absorption data obtained using the Kubelka–Munk function, F(R), for (a) [(CH<sub>3</sub>)<sub>3</sub>SO]Cu<sub>2</sub>I<sub>3</sub>, (b) [(CH<sub>3</sub>)<sub>3</sub>SO]Ag<sub>2</sub>I<sub>3</sub>, (c) [(CH<sub>3</sub>)<sub>3</sub>SO]Cu<sub>1.80(1)</sub>Ag<sub>0.20(1)</sub>I<sub>3</sub>, and (d) [(CH<sub>3</sub>)<sub>3</sub>SO]Cu<sub>0.75(1)</sub>Ag<sub>1.25(1)</sub>I<sub>3</sub>.

To gain a deeper understanding of the optical properties of these materials, we performed diffuse reflectance measurements on polycrystalline powder samples (Figure 4 and S6). The parent compounds [(CH<sub>3</sub>)<sub>3</sub>SO]Cu<sub>2</sub>I<sub>3</sub> and [(CH<sub>3</sub>)<sub>3</sub>SO]Ag<sub>2</sub>I<sub>3</sub> display absorption onsets at ~3.6 eV (Figure 4). In comparison, the reported bandgaps for CsCu<sub>2</sub>I<sub>3</sub> and CsAg<sub>2</sub>I<sub>3</sub> range from 3.4 to 3.65 eV,<sup>7, 28, 33</sup> suggesting that the bandgaps in [(CH<sub>3</sub>)<sub>3</sub>SO]Cu<sub>2</sub>I<sub>3</sub> and [(CH<sub>3</sub>)<sub>3</sub>SO]Ag<sub>2</sub>I<sub>3</sub> are also determined by the inorganic anionic chains. Note that the bandgaps for the alloyed compositions do not follow the linear trend (Figure S6); the estimated band gaps of 3.49 and 3.48 eV for [(CH<sub>3</sub>)<sub>3</sub>SO]Cu<sub>1.80(1)</sub>Ag<sub>0.20(1)</sub>I<sub>3</sub> and [(CH<sub>3</sub>)<sub>3</sub>SO]Cu<sub>0.75(1)</sub>Ag<sub>1.25(1)</sub>I<sub>3</sub> (Figure 4), are lower than 3.63 and 3.57 eV estimated for parents [(CH<sub>3</sub>)<sub>3</sub>SO]Cu<sub>2</sub>I<sub>3</sub> and [(CH<sub>3</sub>)<sub>3</sub>SO]Ag<sub>2</sub>I<sub>3</sub>, respectively. The anomalous bandgap trend is in fact known in many halide perovskites,<sup>43</sup> and in the present case, especially

given the fact that structural parameters also show irregularity, the deviation from Vegard's law in title compounds is understandable. Given that the bandgaps in this family are determined by the polyanionic [M<sub>2</sub>I<sub>3</sub>]<sup>-</sup> chains (see computational results below), the enhanced lattice distortions induced by alloying can lead to changes in the electronic band structure and thus affect the band gap.

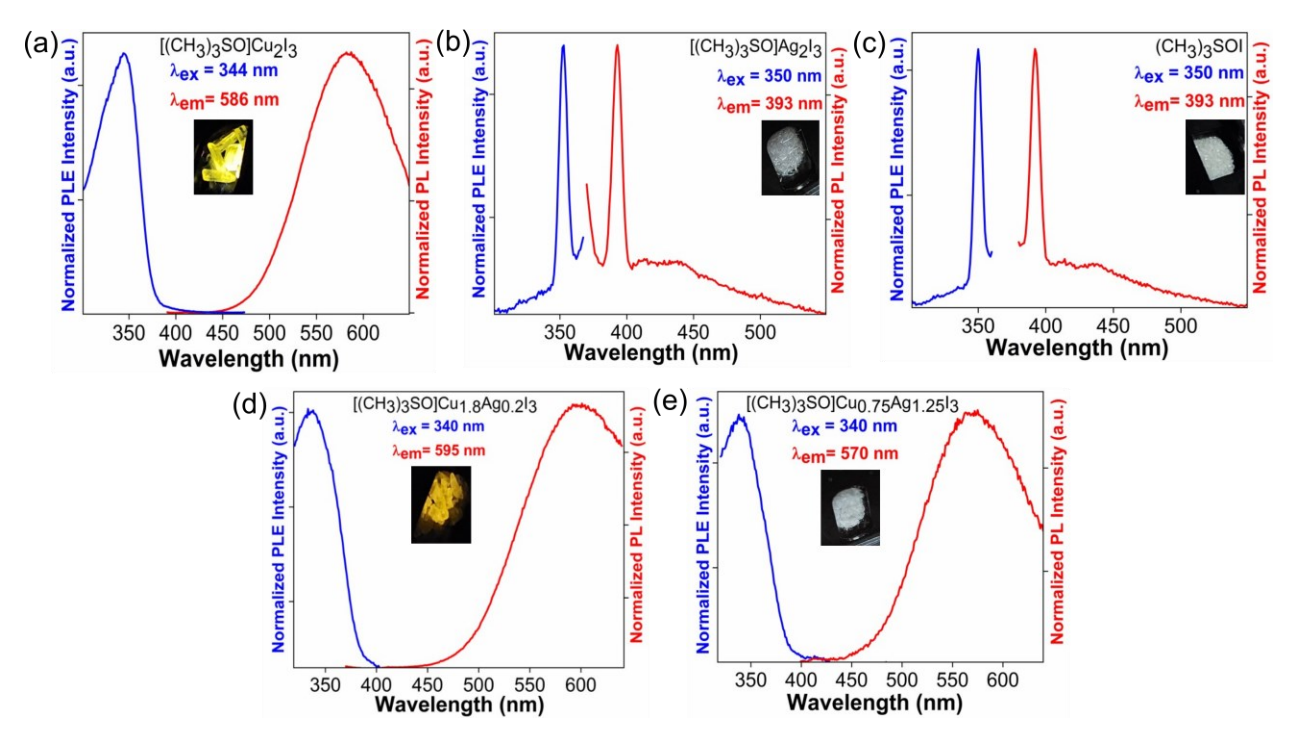


**Figure 5.** Photoluminescence excitation (PLE) (blue) and photoluminescence emission (PL) (red) spectra at room temperature: (a) [(CH<sub>3</sub>)<sub>3</sub>SO]Cu<sub>2</sub>I<sub>3</sub>, (b) [(CH<sub>3</sub>)<sub>3</sub>SO]Ag<sub>2</sub>I<sub>3</sub>, (c) (CH<sub>3</sub>)<sub>3</sub>SO], (d) [(CH<sub>3</sub>)<sub>3</sub>SO]Cu<sub>1.80(1)</sub>Ag<sub>0.20(1)</sub>I<sub>3</sub>, and (e) [(CH<sub>3</sub>)<sub>3</sub>SO]Cu<sub>0.75(1)</sub>Ag<sub>1.25(1)</sub>I<sub>3</sub>. The insets show the light emission of the corresponding compound under UV radiation.

Photoluminescence excitation (PLE) and emission (PL) spectra of the title compounds are presented in Figure 5. It is noteworthy that isostructural title compounds show distinct photophysical properties depending on their compositions. Compound [(CH<sub>3</sub>)<sub>3</sub>SO]Cu<sub>2</sub>I<sub>3</sub> shows an emission band centered at 586 nm for the excitation wavelength of 344 nm with a large Stokes shift of 242 nm, which is comparable to the reported yellow emitter CsCu<sub>2</sub>I<sub>3</sub>, which shows the emission at 576 nm, with a Stokes shift of 242 nm.<sup>7</sup> Therefore, PLE in [(CH<sub>3</sub>)<sub>3</sub>SO]Cu<sub>2</sub>I<sub>3</sub> is assigned to bandgap excitation and PL in [(CH<sub>3</sub>)<sub>3</sub>SO]Cu<sub>2</sub>I<sub>3</sub> can be attributed to self-trapped excitonic (STE) emission localized around copper(I), similar to that in CsCu<sub>2</sub>I<sub>3</sub> and other luminescent copper(I) metal halides.<sup>3, 7, 12, 13, 15, 45, 46</sup> Single crystals of [(CH<sub>3</sub>)<sub>3</sub>SO]Ag<sub>2</sub>I<sub>3</sub> show an emission peak at 393 nm for the excitation wavelength of 350 nm corresponding to the bandgap excitation. These values significantly differ from that reported for the STE-based broadband emitter

CsAq₂l₃, for which PLE<sub>max</sub> is at ≈295 nm and PL is centered at 610 nm. Instead, the PL and PLE characteristics of [(CH<sub>3</sub>)<sub>3</sub>SO]Ag<sub>2</sub>I<sub>3</sub> are like that of the precursor organic salt (CH<sub>3</sub>)<sub>3</sub>SOI. In [(CH<sub>3</sub>)<sub>3</sub>SO]Ag<sub>2</sub>I<sub>3</sub>, UV light photoexcites the organic structural component leading to the organic molecular emission. This observation suggests that (i) the organic states are very close to the band edges (see computational results below) and (ii) introduction of silver ions in the compound quenches the inorganic emission. The latter observation matches with the fact that Ag(I) analogs of high-efficiency Cu(I) halides are known to have much lower PL emission efficiencies (often, completely guenched PL).<sup>2</sup> Interestingly, the alloyed compositions [(CH<sub>3</sub>)<sub>3</sub>SO]Cu<sub>1.80(1)</sub>Ag<sub>0.20(1)</sub>I<sub>3</sub>  $[(CH_3)_3SO]Cu_{0.75(1)}Ag_{1.25(1)}I_3 \quad display \quad PL/PLE \quad characteristics \quad similar \quad to \quad that \quad of \quad all \quad$ [(CH<sub>3</sub>)<sub>3</sub>SO]Cu<sub>2</sub>l<sub>3</sub> with PLE peaks at 340 nm, and a broadband PL emission peaks centered at 595 nm and 570 nm, respectively. Given the PL/PLE data for alloyed compositions, we attribute their Stokes-shifted broadband light emission to STE emission.7, 12, 32, 47-49 Importantly, unlike other STE-based Cu(I) halide emitters, title compounds display very dim emissions with PLQYs below 1%. On the one hand, this is unsurprising given the lowest emission efficiency of the CsCu<sub>2</sub>l<sub>3</sub> parent among the alkali halides.<sup>2</sup> On the other hand, the incorporation of larger organic cations in place of Cs<sup>+</sup> to increase charge localization in [M<sub>2</sub>I<sub>3</sub>]<sup>-</sup> chains and alloying experiments were performed to boost the emission efficiency of the "123" family. Nevertheless, these results can be rationalized by considering the fact that only minor structural changes occur in the title compounds as compared to that of CsCu<sub>2</sub>l<sub>3</sub> and CsAg<sub>2</sub>l<sub>3</sub>, which also have very weak PL emission properties. Other contributing factors could include the detrimental defect properties of Ag-containing compositions, e.g., Ag(I) iodides have been studied as ionic and superionic conductors in the past hundred years.<sup>2, 50</sup> In fact, the Cu-Ag alloyed compositions are likely to exhibit even poorer defect properties. Indeed, the past research on the "123" family has shown that halide alloyed compositions CsCu<sub>2</sub>Cl<sub>1.5</sub>Br<sub>1.5</sub> and CsCu<sub>2</sub>Br<sub>1.5</sub>I<sub>1.5</sub> also have quenched PL with efficiencies below 1%.

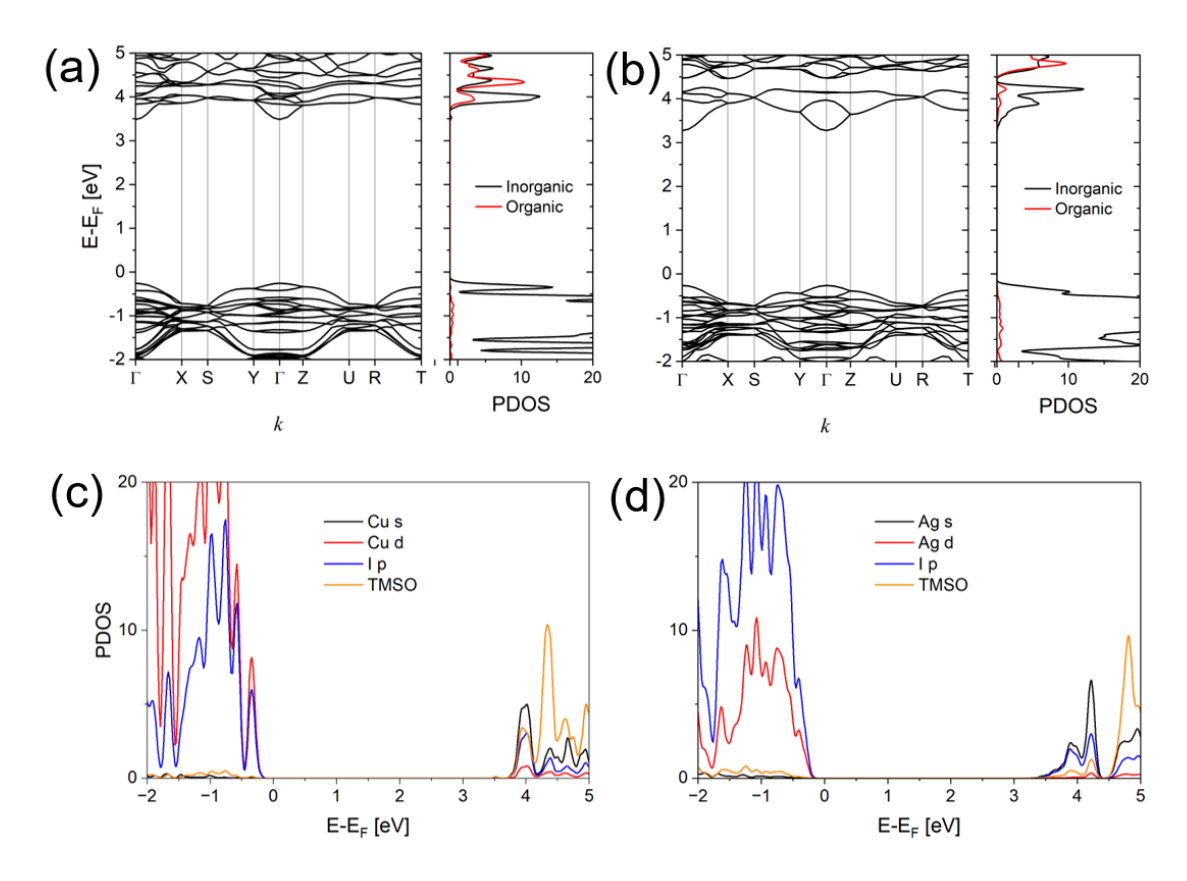


**Figure 6.** Band structures and contributions of organic and inorganic states for (a)  $[(CH_3)_3SO]Cu_2l_3$  and (b)  $[(CH_3)_3SO]Ag_2l_3$ . Projected density of states (PDOS) plots for (c)  $[(CH_3)_3SO]Cu_2l_3$  and (d)  $[(CH_3)_3SO]Ag_2l_3$ . TMSO denotes the trimethylsulfoxonium  $(CH_3)_3SO^+$ .

The calculated bandgaps using the range separated hybrid functional HSE06 are 3.74 eV for [(CH<sub>3</sub>)<sub>3</sub>SO]Cu<sub>2</sub>I<sub>3</sub> and 3.54 eV for [(CH<sub>3</sub>)<sub>3</sub>SO]Ag<sub>2</sub>I<sub>3</sub>, respectively, in agreement with the experimentally estimated optical gaps (Figure 4). The calculated band structures and projected density of states (PDOS) in Figure 6(a, b) show that the band dispersions are stronger along the 1D axis direction, i.e., along ΓX, SY, ZU, and RT. The PDOS indicates that the DOS of the organic part is weak near the valence band maximum (VBM), unlike the DOS from the inorganic component. Near the conduction band minimum (CBM) however, the DOS of the inorganic and organic parts occur at about the same energies for [(CH<sub>3</sub>)<sub>3</sub>SO]Cu<sub>2</sub>I<sub>3</sub>, with a larger DOS for the organic component. On the other hand, for [(CH<sub>3</sub>)<sub>3</sub>SO]Ag<sub>2</sub>I<sub>3</sub> the electronic states from the organic cation are slightly above the states from the inorganic component near the CBM. But the primary contribution to the systems' VBM-CBM band gap originates from the inorganic component. A detailed examination of the orbital contributions to the PDOS shown in Figure 6 indicates that the VBM of the inorganic component is from Cu or Ag *d* and I *p* orbitals, and the CBM of the inorganic component is from Cu or Ag *s* and I *p* orbitals.

These results agree with the reported band structures of analogous Cu(I) and Ag(I) halides.<sup>2</sup>

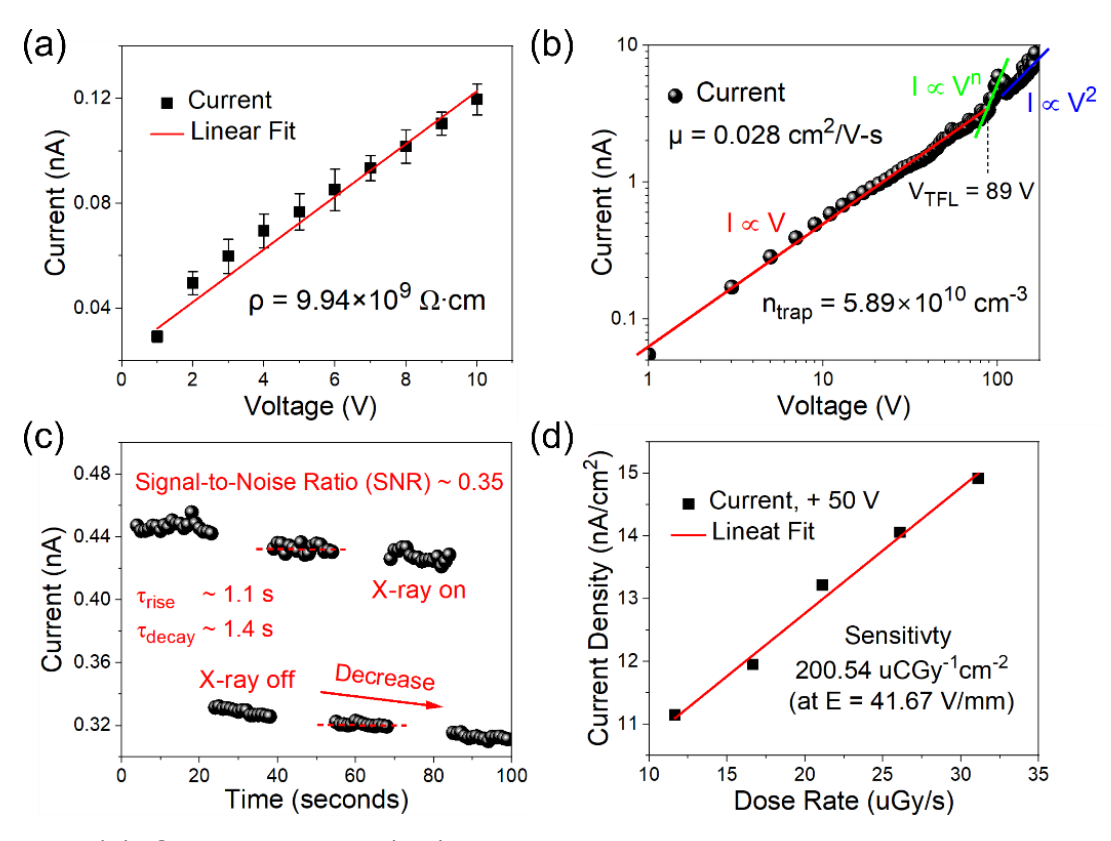


**Figure 7.** (a) Current-voltage (I-V) curve measured to determine the semiconductor resistivity of [(CH<sub>3</sub>)<sub>3</sub>SO]Cu<sub>2</sub>I<sub>3</sub>. (b) Space-charge-limited-current measurement for evaluating the density of trap levels in as-grown [(CH<sub>3</sub>)<sub>3</sub>SO]Cu<sub>2</sub>I<sub>3</sub> single crystals. (c) X-ray 'on' and 'off' measurement. The signal-to-noise (SNR) ratio and rise/decay time were extracted from the measurement. (d) Measured X-ray detection sensitivity for the fabricated prototype X-ray detector.

In literature, copper(I) and silver(I) halides have been considered for optical, electrical and radiation detection applications.  $^{2, 26, 51-54}$  Although the weak light emission properties of the title compounds preclude their use as scintillator materials, we considered their potential use in semiconductor direct conversion X-ray radiation detector applications with [(CH<sub>3</sub>)<sub>3</sub>SO]Cu<sub>2</sub>I<sub>3</sub> as the representative of the family. Figure 7a shows the current-voltage (I-V) curve measured using a single crystal of [(CH<sub>3</sub>)<sub>3</sub>SO]Cu<sub>2</sub>I<sub>3</sub>. The bulk crystal resistivity is calculated to be  $9.94\times10^9~\Omega\cdot\text{cm}$ , which is ideal for reducing the detector leakage current for detection applications and is comparable to that for leading room-temperature cadmium zinc telluride (CZT) semiconductor detector material  $4.5\times10^{10}~\Omega\cdot\text{cm}$ . Figure 7b is the space-charge-limited-current (SCLC) measurement for evaluating the density of trap states and carrier mobility of as-grown single crystal of

[(CH<sub>3</sub>)<sub>3</sub>SO]Cu<sub>2</sub>I<sub>3</sub>. In the measured SCLC curve, there are three current transition regimes, Ohmic (I $\propto$ V), trap-filled-limited (I $\propto$ V<sup>n</sup>), and Child (I $\propto$ V<sup>2</sup>). The density of trap states is estimated from the trap-filled-limited (TFL) regime using the formula below,<sup>56</sup>

$$n_{trap} = \frac{2\epsilon\epsilon_0}{eL^2} V_{TFL}$$

where  $n_{trap}$  is the density of trap states (cm<sup>-3</sup>),  $\epsilon$  is the dielectric constant (= 13.47),  $\epsilon_0$  is the vacuum permittivity, e is the electronic charge, L is the crystal thickness (= 0.15 cm), and  $V_{TFL}$  (= 89 V) is the onset voltage of the TFL regime. For [(CH<sub>3</sub>)<sub>3</sub>SO]Cu<sub>2</sub>I<sub>3</sub>, the trap level is estimated to be 5.89×10<sup>10</sup> cm<sup>-3</sup>, which is close to the reported results for other metal halides,  $10^9$ - $10^{10}$  cm<sup>-3</sup> for MAPbBr<sub>3</sub> and  $3.33\times10^{10}$  cm<sup>-3</sup> for Rb<sub>4</sub>Ag<sub>2</sub>BiBr<sub>9</sub>.<sup>57, 58</sup> The carrier mobility of [(CH<sub>3</sub>)<sub>3</sub>SO]Cu<sub>2</sub>I<sub>3</sub> is determined from the Child regime according to the Mott-Gurney law,<sup>59</sup>

$$\mu = \frac{8J_D L^3}{9\varepsilon\varepsilon_0 V^2}$$

where  $J_D$  is the current density at applied voltage V and  $\mu$  is the carrier mobility. For  $[(CH_3)_3SO]Cu_2l_3$ , a low mobility value of ~0.03 cm<sup>2</sup>/V-s was found.

To further demonstrate the potential of using the "123" compounds for X-ray detection applications, we fabricated a prototype X-ray detector using a single crystal of  $[(CH_3)_3SO]Cu_2I_3$ . The prototype detector was then exposed to soft X-rays produced from a Cu X-ray tube. Figure 7c is the X-ray 'on' and 'off' measurements, which clearly shows that  $[(CH_3)_3SO]Cu_2I_3$ -based detector is responsive to soft X-ray photons with a signal-tonoise (SNR) ratio (where SNR =  $\frac{I_{x-ray\,on}-I_{x-ray\,off}}{I_{x-ray\,off}}$ ) of ~0.35. The X-ray induced current signal rise time and decay time is determined to be ~1.1 s and ~1.4 s (measured from 10% to 90% of the current amplitude), respectively. As can be observed from Figure 7c, the recorded current decreased slightly over the measurement period. This can be ascribed to the ionic migration of halogen ions, which is a typical observation for halide semiconductors. For the fabricated detector, a detection sensitivity of 200.54 uCGy-1cm-2 (at electrical field E=41.67 V/mm) was obtained (Figure 7d). The determined sensitivity of  $[(CH_3)_3SO]Cu_2I_3$  is comparable to a recently reported two-dimensional halide Rb4Ag2BiBr9 (222.03 uCGy-1cm-2 at E=24 V/mm) and much better than that for zero-dimensional halide FA3Bi2I9 (598.1 uCGy-1cm-2 at E=555 V/mm).

## 4. Conclusion

In summary, this study reports the preparation and physical properties of new hybrid metal halides in the "123" family,  $[(CH_3)_3SO]M_2I_3$  (where M = Cu, Ag). These halides feature 1D crystal structures containing  $[M_2X_3]^-$  anionic double chains made of

edge-sharing MX<sub>4</sub> tetrahedra. The anionic [M<sub>2</sub>X<sub>3</sub>]<sup>-</sup> are separated by (CH<sub>3</sub>)<sub>3</sub>SO<sup>+</sup> cations, however, this separation is only slightly longer than that observed for the all-inorganic analogs CsM<sub>2</sub>I<sub>3</sub>. Furthermore, computational results suggest that the orbital contributions to the states around the bandgap for [(CH<sub>3</sub>)<sub>3</sub>SO]M<sub>2</sub>I<sub>3</sub> are similar to that reported for CsM<sub>2</sub>I<sub>3</sub>. Consequently, the obtained optical spectroscopy measurement results for [(CH<sub>3</sub>)<sub>3</sub>SO]M<sub>2</sub>I<sub>3</sub> are also similar to that of their all-inorganic counterparts – their estimated band gaps are at ~3.6 eV. Moreover, PLQY values estimated for [(CH<sub>3</sub>)<sub>3</sub>SO]M<sub>2</sub>I<sub>3</sub> are also very low (<1%), mirroring the record low emission efficiency for an all-inorganic Cu(I) halide reported for CsCu<sub>2</sub>I<sub>3</sub>. The Cu-Ag alloyed compositions are found to be equally weak emitters, also attributed to a surprisingly potent charge delocalization observed in the "123" compounds. Interestingly, both Cu site (this work) and halide site alloying of CsCu<sub>2</sub>I<sub>3</sub> has now been accomplished, yielding quenched PL in both cases, which suggests that the increased defect concentration due to alloying may also be a contributing factor in PL quenching. Given their very low emission efficiencies, the utilization of [(CH<sub>3</sub>)<sub>3</sub>SO]M<sub>2</sub>I<sub>3</sub> in optical applications is unlikely unless an engineering approach can be developed to boost their emission efficiencies such as the host-dopant strategy used for CsCu<sub>2</sub>l<sub>3</sub> used in LEDs.<sup>25</sup> Instead, we find that [(CH<sub>3</sub>)<sub>3</sub>SO]M<sub>2</sub>l<sub>3</sub> may have potential for use in semiconductor direct conversion X-ray detection applications. Important conclusion from this work, to improve the PLQYs of the "123" compounds via chemical modifications, even larger organic cations may need to be incorporated to induce a stronger charge localization and enhance the probability of formation of roomtemperature stable excitons.

# Associated Content Supporting Information

The Supporting Information is available free of charge at <a href="http://pubs.acs.org">http://pubs.acs.org</a>

Single crystal data and structure refinement parameters for  $[(CH_3)_3SO]Cu_{2-x}Ag_xI_3$  (experimental x=0, 0.2, 1.25, 2, respectively), atomic coordinates and equivalent isotropic displacement parameters for  $[(CH_3)_3SO]Cu_{2-x}Ag_xI_3$  (experimental x=0, 0.2, 1.25, 2, respectively), photographs of the synthesized crystals, coordination environment of metal halide tetrahedra in  $[(CH_3)_3SO]Cu_{2-x}Ag_xI_3$  (experimental x=0, 0.2, 1.25, 2, respectively), periodic PXRD measurement, PXRD measurements for  $[(CH_3)_3SO]Cu_{2-x}Ag_xI_3$  (nominal x=0, 0.2, 0.4, 1, 1.4, 2), Vegard's plot, diffuse reflectance data for all compounds, SEM images and elemental mapping images, and metal halide composition analysis from EDS measurements (PDF)

### **Author information**

### **Corresponding Author**

Bayram Saparov – Department of Chemistry & Biochemistry, University of Oklahoma, Norman, Oklahoma 73019-5251, United States; <a href="https://orcid.org/0000-0003-0190-9585">https://orcid.org/0000-0003-0190-9585</a>; Email: <a href="mailto:saparov@ou.edu">saparov@ou.edu</a>

#### **Authors**

Tamanna Pinky – Department of Chemistry & Biochemistry, University of Oklahoma, Norman, Oklahoma 73019-5251, United States

Dilruba A. Popy – Department of Chemistry & Biochemistry, University of Oklahoma, Norman, Oklahoma 73019-5251, United States

Zheng Zhang – Department of Chemistry, Tulane University, New Orleans, LA 70118, United States

Jie Jiang – Air Force Research Laboratory, Materials and Manufacturing Directorate, Wright-Patterson Air Force Base, Ohio 45433, United States

Ruth Pachter – Air Force Research Laboratory, Materials and Manufacturing Directorate, Wright-Patterson Air Force Base, Ohio 45433, United States

#### **Notes**

The authors declare that they have no known competing financial interests or personal relationships that could have appeared to influence the work reported in this paper.

### Acknowledgement

This research received funding support from National Science Foundation under award number NSF DMR-2045490. We thank Dr. Douglas Powel for his assistance in conducting SCXRD measurements, which was made possible by the NSF grant CHE-1726630. X-ray response tests were carried out using the Biomolecular Structure Core (BSC)-Norman facility. The BSC-Norman is supported in part by Institutional Development Award (IDeA) from the National Institute of General Medical Sciences of the National Institutes of Health (award P20GM103640 and award P30GM145423), the National Science Foundation (award 0922269), and the University of Oklahoma Department of Chemistry and Biochemistry. Authors would like to thank Dr. Leonard Thomas for his kind help with the X-ray response measurements. Microscopy data collection was performed at the Samuel Roberts Noble Microscopy Laboratory with the help from Dr. Preston Larson.

### References

- (1) Xing, X.; Tong, T.; Mohebinia, M.; Wang, D.; Ren, Z.; Hadjiev, V. G.; Wang, Z.; Bao, J. Photoluminescence and Raman Spectra of One-Dimensional Lead-free Perovskite CsCu2l3 Single-Crystal Wires. *J. Phys. Chem. Lett.* **2022**, *13* (28), 6447-6454.
- (2) Banerjee, D.; Saparov, B. Ultrabright Light Emission Properties of All-Inorganic and Hybrid Organic–Inorganic Copper(I) Halides. *Chem. Mater.* **2023**, *35* (9), 3364-3385.
- (3) Creason, T. D.; McWhorter, T. M.; Bell, Z.; Du, M.-H.; Saparov, B. K<sub>2</sub>CuX<sub>3</sub> (X = Cl, Br): All-Inorganic Lead-Free Blue Emitters with Near-Unity Photoluminescence Quantum Yield. *Chem. Mater.* **2020**, *32* (14), 6197-6205.
- (4) Koh, T. M.; Shanmugam, V.; Schlipf, J.; Oesinghaus, L.; Müller-Buschbaum, P.; Ramakrishnan, N.; Swamy, V.; Mathews, N.; Boix, P. P.; Mhaisalkar, S. G. Nanostructuring mixed-dimensional perovskites: a route toward tunable, efficient photovoltaics. *Adv. Mater.* **2016**, *28* (19), 3653-3661.
- (5) Ma, Z.; Ji, X.; Lin, S.; Chen, X.; Wu, D.; Li, X.; Zhang, Y.; Shan, C.; Shi, Z.; Fang, X. Recent Advances and Opportunities of Eco-Friendly Ternary Copper Halides: A New Superstar in Optoelectronic Applications. *Adv. Mater.* **2023**, 2300731.
- (6) Creason, T. D.; Yangui, A.; Roccanova, R.; Strom, A.; Du, M.-H.; Saparov, B. Rb2CuX3 (X = Cl, Br): 1D All-Inorganic Copper Halides with Ultrabright Blue Emission and Up-Conversion Photoluminescence. *Adv. Opt. Mater.* **2020**, *8* (2), 1901338.
- (7) Roccanova, R.; Yangui, A.; Seo, G.; Creason, T. D.; Wu, Y.; Kim, D. Y.; Du, M.-H.; Saparov, B. Bright Luminescence from Nontoxic CsCu2X3 (X = Cl, Br, I). *ACS Mater. Lett.* **2019**, *1* (4), 459-465.
- (8) Li, J.; Inoshita, T.; Ying, T.; Ooishi, A.; Kim, J.; Hosono, H. A Highly Efficient and Stable Blue-Emitting Cs5Cu3Cl6I2 with a 1D Chain Structure. *Adv. Mater.* **2020**, *32* (37), 2002945.
- (9) Roccanova, R.; Yangui, A.; Nhalil, H.; Shi, H.; Du, M.-H.; Saparov, B. Near-Unity Photoluminescence Quantum Yield in Blue-Emitting Cs3Cu2Br5–xlx ( $0 \le x \le 5$ ). ACS Appl. Electron. Mater. **2019**, *1* (3), 269-274.
- (10) Du, M.-H. Emission Trend of Multiple Self-Trapped Excitons in Luminescent 1D Copper Halides. *ACS Energy Lett.* **2020**, *5* (2), 464-469.

- (11) Li, Y.; Vashishtha, P.; Zhou, Z.; Li, Z.; Shivarudraiah, S. B.; Ma, C.; Liu, J.; Wong, K. S.; Su, H.; Halpert, J. E. Room temperature synthesis of stable, printable Cs3Cu2X5 (X= I, Br/I, Br, Br/Cl, Cl) colloidal nanocrystals with near-unity quantum yield green emitters (X= Cl). *Chem. Mater.* **2020**, 32 (13), 5515-5524.
- (12) Peng, H.; Yao, S.; Guo, Y.; Zhi, R.; Wang, X.; Ge, F.; Tian, Y.; Wang, J.; Zou, B. Highly efficient self-trapped exciton emission of a (MA) 4Cu2Br6 single crystal. *J. Phys. Chem. Lett.* **2020**, *11* (12), 4703-4710.
- (13) Peng, H.; Tian, Y.; Wang, X.; Dong, T.; Yu, Z.; Xiao, Y.; Zhang, Z.; Wang, J.; Zou, B. Highly efficient broadband green emission of (TPA) CuCl2 single crystals: understanding the formation of self-trapped states. *J. Phys. Chem. C* **2022**, *126* (19), 8545-8552.
- (14) Peng, H.; Wang, X.; Tian, Y.; Zou, B.; Yang, F.; Huang, T.; Peng, C.; Yao, S.; Yu, Z.; Yao, Q. Highly efficient cool-white photoluminescence of (Gua) 3Cu2l5 single crystals: formation and optical properties. *ACS Appl. Mater. Interfaces* **2021**, *13* (11), 13443-13451.
- (15) Peng, H.; Tian, Y.; Wang, X.; Huang, T.; Xiao, Y.; Dong, T.; Hu, J.; Wang, J.; Zou, B. Bulk assembly of a 0D organic antimony chloride hybrid with highly efficient orange dual emission by self-trapped states. *J. Mater. Chem. C* **2021**, *9* (36), 12184-12190, 10.1039/D1TC02906A.
- (16) Popy, D. A.; Creason, T. D.; Zhang, Z.; Singh, D. J.; Saparov, B. Electronic structures and optical properties of (Ph4P) MX2 (M= Cu, Ag; X= Cl, Br). *J. Solid State Chem.* **2022**, *316*, 123626.
- (17) Lian, L.; Wang, S.; Ding, H.; Liang, G.; Zhao, Y.-B.; Song, H.; Lan, X.; Gao, J.; Chen, R.; Zhang, D.; et al. Single-Component White-Light Emitters with Excellent Color Rendering Indexes and High Photoluminescence Quantum Efficiencies. *Adv. Opt. Mater.* **2022**, *10* (1), 2101640.
- (18) Lin, R.; Guo, Q.; Zhu, Q.; Zhu, Y.; Zheng, W.; Huang, F. All-Inorganic CsCu2l3 Single Crystal with High-PLQY (≈15.7%) Intrinsic White-Light Emission via Strongly Localized 1D Excitonic Recombination. *Adv. Mater.* **2019**, *31* (46), 1905079.
- (19) Li, Y.; Shi, Z.; Wang, L.; Chen, Y.; Liang, W.; Wu, D.; Li, X.; Zhang, Y.; Shan, C.; Fang, X. Solution-processed one-dimensional CsCu 2 I 3 nanowires for polarization-sensitive and flexible ultraviolet photodetectors. *Mater. Horiz.* **2020**, *7* (6), 1613-1622.
- (20) Mo, X.; Li, T.; Huang, F.; Li, Z.; Zhou, Y.; Lin, T.; Ouyang, Y.; Tao, X.; Pan, C. Highly-efficient all-inorganic lead-free 1D CsCu2I3 single crystal for white-light emitting diodes and UV photodetection. *Nano Energy* **2021**, *81*, 105570.

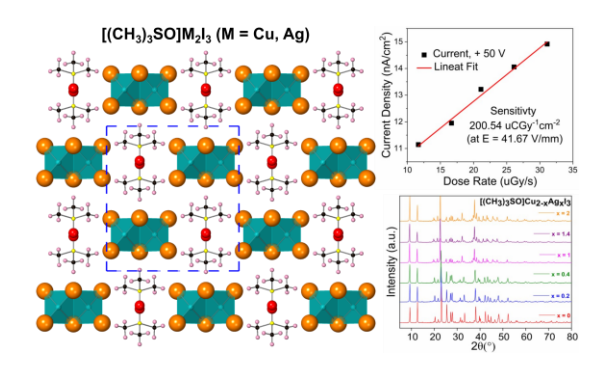
- (21) Cheng, S.; Beitlerova, A.; Kucerkova, R.; Mihokova, E.; Nikl, M.; Zhou, Z.; Ren, G.; Wu, Y. Non-hygroscopic, self-absorption free, and efficient 1D CsCu2l3 perovskite single crystal for radiation detection. *ACS Appl. Mater. Interfaces* **2021**, *13* (10), 12198-12202.
- (22) Liu, W.; Ng, K. W.; Lin, H.; Dai, Z.; Xu, J.; Su, S.; Tang, Z.; Wang, S. Stable UV-pumped white light-emitting diodes based on anthracene-coated CsCu2l3. *J. Phys. Chem. C* **2021**, *125* (23), 13076-13083.
- (23) Zhang, M.; Zhu, J.; Yang, B.; Niu, G.; Wu, H.; Zhao, X.; Yin, L.; Jin, T.; Liang, X.; Tang, J. Oriented-structured CsCu2l3 film by close-space sublimation and nanoscale seed screening for high-resolution X-ray imaging. *Nano Lett.* **2021**, *21* (3), 1392-1399.
- (24) Li, Z.; Li, Z.; Shi, Z.; Fang, X. Facet-Dependent, Fast Response, and Broadband Photodetector Based on Highly Stable All-Inorganic CsCu2l3 Single Crystal with 1D Electronic Structure. *Adv. Funct. Mater.* **2020**, *30* (28), 2002634.
- (25) Seo, G.; Jung, H.; Creason, T. D.; Yeddu, V.; Bamidele, M.; Echeverria, E.; Lee, J.; McIlroy, D.; Saparov, B.; Kim, D. Y. Lead-Free Halide Light-Emitting Diodes with External Quantum Efficiency Exceeding 7% Using Host–Dopant Strategy. *ACS Energy Lett.* **2021**, 6 (7), 2584-2593.
- (26) van Blaaderen, J. J.; van den Brekel, L. A.; Krämer, K. W.; Dorenbos, P. Scintillation and Optical Characterization of CsCu2l3 Single Crystals from 10 to 400 K. *Chem. Mater.* **2023**, *35* (22), 9623-9631.
- (27) Yue, C.-Y.; Lin, N.; Gao, L.; Jin, Y.-X.; Liu, Z.-Y.; Cao, Y.-Y.; Han, S.-S.; Lian, X.-K.; Hu, B.; Lei, X.-W. Organic cation directed one-dimensional cuprous halide compounds: syntheses, crystal structures and photoluminescence properties. *Dalton Trans.* **2019**, *48* (27), 10151-10159.
- (28) Yao, M.-M.; Zhang, Q.; Wang, D.; Chen, R.-I.; Yin, Y.-C.; Xia, J.; Tang, H.; Xu, W.-P.; Yu, S.-H. Lead-Free Halide CsAg2I3 with 1D Electronic Structure and High Stability for Ultraviolet Photodetector. *Adv. Funct. Mater.* **2022**, 32 (28), 2202894.
- (29) Brink, C.; Binnendijk, N. F.; Van De Linde, J. The crystal structures of CsCu2Cl3 and CsAg2l3. *Acta Cryst.* **1954**, *7* (2), 176-180.
- (30) Hull, S.; Berastegui, P. Crystal Structures and Ionic Conductivities of Ternary Derivatives of the Silver and Copper Monohalides—II: Ordered Phases within the (AgX)<sub>x</sub>–(MX)<sub>1-x</sub> and (CuX)<sub>x</sub>–(MX)<sub>1-x</sub> (M=K, Rb and Cs; X=Cl, Br and I) Systems. *J. Solid State Chem.* **2004**, *177* (9), 3156-3173.

- (31) Kumar, P.; Creason, T. D.; Fattal, H.; Sharma, M.; Du, M.-H.; Saparov, B. Composition-Dependent Photoluminescence Properties and Anti-Counterfeiting Applications of A2AgX3 (A = Rb, Cs; X = Cl, Br, I). *Adv. Funct. Mater.* **2021**, *31* (48), 2104941.
- (32) Creason, T. D.; Fattal, H.; Gilley, I. W.; McWhorter, T. M.; Du, M.-H.; Saparov, B. (NH4)2AgX3 (X = Br, I): 1D Silver Halides with Broadband White Light Emission and Improved Stability. *ACS Mater. Au* **2021**, *1* (1), 62-68.
- (33) Yao, M. M.; Zhang, Q.; Wang, D.; Chen, R. I.; Yin, Y. C.; Xia, J.; Tang, H.; Xu, W. P.; Yu, S. H. Lead-Free Halide CsAg2l3 with 1D Electronic Structure and High Stability for Ultraviolet Photodetector. *Adv. Funct. Mater.* **2022**, *32* (28), 2202894.
- (34) Kresse, G.; Furthmüller, J. Efficiency of ab-initio total energy calculations for metals and semiconductors using a plane-wave basis set. *Comput. Mater. Sci.* **1996**, *6* (1), 15-50.
- (35) Kresse, G.; Joubert, D. From ultrasoft pseudopotentials to the projector augmented-wave method. *Phys. Rev. B* **1999**, *59* (3), 1758.
- (36) Perdew, J. P.; Burke, K.; Ernzerhof, M. Generalized gradient approximation made simple. *Phys. Rev. Lett.* **1996**, *77* (18), 3865.
- (37) Grimme, S.; Antony, J.; Ehrlich, S.; Krieg, H. A consistent and accurate ab initio parametrization of density functional dispersion correction (DFT-D) for the 94 elements H-Pu. *J. Chem. Phys.* **2010**, *132* (15).
- (38) Beck, H.; Gehrmann, C.; Egger, D. A. Structure and binding in halide perovskites: Analysis of static and dynamic effects from dispersion-corrected density functional theory. *APL Mater.* **2019**, *7* (2).
- (39) Zhang, L.; Liang, W. How the structures and properties of two-dimensional layered perovskites MAPbl3 and CsPbl3 vary with the number of layers. *J. Phys. Chem. Lett.* **2017**, *8* (7), 1517-1523.
- (40) Jagner, S.; Helgesson, G. On the coordination number of the metal in crystalline halogenocuprates (I) and halogenoargentates (I). *Adv. Inorg. Chem.* **1991**, *37*, 1-45.
- (41) Kildea, J.; Skelton, B.; White, A. Crystal-Structures of (Nh4) 2 (AgI3)∞/∞. H2O And (Nme4)(Ag2I3)∞/∞. *Aust. J. Chem.* **1986**, *39* (1), 171-175.
- (42) Lehmann, F.; Franz, A.; Többens, D. M.; Levcenco, S.; Unold, T.; Taubert, A.; Schorr, S. The phase diagram of a mixed halide (Br, I) hybrid perovskite obtained by synchrotron X-ray diffraction. *RSC Adv.* **2019**, *9* (20), 11151-11159.

- (43) Mao, L.; Stoumpos, C. C.; Kanatzidis, M. G. Two-dimensional hybrid halide perovskites: principles and promises. *J. Am. Chem. Soc.* **2018**, *141* (3), 1171-1190.
- (44) Roccanova, R.; Ming, W.; Whiteside, V. R.; McGuire, M. A.; Sellers, I. R.; Du, M.-H.; Saparov, B. Synthesis, crystal and electronic structures, and optical properties of (CH3NH3) 2CdX4 (X= Cl, Br, I). *Inorg. Chem.* **2017**, *56* (22), 13878-13888.
- (45) Banerjee, D.; Popy, D. A.; Leininger, B. C.; Creason, T. D.; Mapara, V. N.; Furis, M.; Borunda, M. F.; Saparov, B. Zero-Dimensional Broadband Yellow Light Emitter (TMS) 3Cu2I5 for Latent Fingerprint Detection and Solid-State Lighting. *ACS Appl. Mater. Interfaces* **2023**.
- (46) An, R.; Hao, J.; Song, S.; Zhang, H.; Feng, J.; Wang, X.; Sun, H. Multi-Responsive 0D Organic–Inorganic Hybrid Cuprous Bromides Constructed via Ultra-Facile Approaches for Multimodal Luminescent Anti-Counterfeiting. *Adv. Opt. Mater.* **2023**, *11* (12), 2202596.
- (47) Peng, H.; Tian, Y.; Zhang, Z.; Wang, X.; Huang, T.; Dong, T.; Xiao, Y.; Wang, J.; Zou, B. Bulk assembly of zero-dimensional organic copper bromide hybrid with bright self-trapped exciton emission and high antiwater stability. *J. Phys. Chem. C* **2021**, *125* (36), 20014-20021.
- (48) Xu, T.; Li, Y.; Nikl, M.; Kucerkova, R.; Zhou, Z.; Chen, J.; Sun, Y.-Y.; Niu, G.; Tang, J.; Wang, Q. Lead-free zero-dimensional organic-copper (I) halides as stable and sensitive X-ray scintillators. *ACS Appl. Mater. Inerfaces* **2022**, *14* (12), 14157-14164.
- (49) Peng, H.; Zou, B. Effects of Electron–Phonon Coupling and Spin–Spin Coupling on the Photoluminescence of Low-Dimensional Metal Halides. *J. Phys. Chem. Lett.* **2022**, *13* (7), 1752-1764.
- (50) Rodríguez, L.; Zapata, J.; Vargas, R.; Lara, D. P.; Diosa, J. Superionic behavior in the xAgI–(1- x) CsAg2I3 polycrystalline system. *J. Phys. Chem. Solids* **2016**, 93, 126-130.
- (51) Cheng, S.; Nikl, M.; Beitlerova, A.; Kucerkova, R.; Du, X.; Niu, G.; Jia, Y.; Tang, J.; Ren, G.; Wu, Y. Ultrabright and Highly Efficient All-Inorganic Zero-Dimensional Perovskite Scintillators. *Adv. Opt. Mater.* **2021**, *9* (13), 2100460.
- (52) Liu, Y.-H.; Wang, N.-N.; Ren, M.-P.; Yan, X.; Wu, Y.-F.; Yue, C.-Y.; Lei, X.-W. Zero-Dimensional Hybrid Cuprous Halide of [BAPMA]Cu2Br5 as a Highly Efficient Light Emitter and an X-Ray Scintillator. *ACS Appl. Mater. Interfaces* **2023**, *15* (16), 20219-20227.

- (53) Lin, N.; Wang, R.-C.; Zhang, S.-Y.; Lin, Z.-H.; Chen, X.-Y.; Li, Z.-N.; Lei, X.-W.; Wang, Y.-Y.; Yue, C.-Y. 0D Hybrid Cuprous Halide as an Efficient Light Emitter and X-Ray Scintillator. *Laser Photonics Rev. n/a* (n/a), 2300427.
- (54) Li, D.-Y.; Wu, J.-H.; Wang, X.-Y.; Zhang, X.-Y.; Yue, C.-Y.; Lei, X.-W. Reversible Triple-Mode Photo-and Radioluminescence and Nonlinear Optical Switching in Highly Efficient 0D Hybrid Cuprous Halides. *Chem. Mater.* **2023**, *35* (17), 6598-6611.
- (55) De Antonis, P.; Morton, E.; Menezes, T. Measuring the bulk resistivity of CdZnTe single crystal detectors using a contactless alternating electric field method. *Nucl. Instru. Meth. A* **1996**, *380* (1-2), 157-159.
- (56) Bube, R. H. Trap density determination by space-charge-limited currents. *J. Appl. Phys.* **1962**, 33 (5), 1733-1737.
- (57) Pospisil, J.; Zmeskal, O.; Nespurek, S.; Krajcovic, J.; Weiter, M.; Kovalenko, A. Density of bulk trap states of hybrid lead halide perovskite single crystals: temperature modulated space-charge-limited-currents. *Sci. Rep.* **2019**, *9* (1), 3332.
- (58) Zhang, Z.; Ma, Y.-Z.; Thomas, L.; Gofryk, K.; Saparov, B. Physical properties of candidate X-ray detector material Rb4Ag2BiBr9. *Cryst. Growth Des.* **2021**, *22* (2), 1066-1072.
- (59) De Boer, R.; Jochemsen, M.; Klapwijk, T.; Morpurgo, A.; Niemax, J.; Tripathi, A.; Pflaum, J. Space charge limited transport and time of flight measurements in tetracene single crystals: A comparative study. *J. Appl. Phys.* **2004**, *95* (3), 1196-1202.
- (60) Leao, C. R.; Lordi, V. Simultaneous control of ionic and electronic conductivity in materials: thallium bromide case study. *Phys. Rev. Lett.* **2012**, *108* (24), 246604.
- (61) Li, W.; Xin, D.; Tie, S.; Ren, J.; Dong, S.; Lei, L.; Zheng, X.; Zhao, Y.; Zhang, W.-H. Zero-dimensional lead-free FA3Bi2I9 single crystals for high-performance X-ray detection. *J. Phys. Chem. Lett.* **2021**, *12* (7), 1778-1785.

# For Table of Contents:



<u>Synopsis:</u> This study reports the preparation and characterization of new hybrids  $[(CH_3)_3SO]M_2I_3$  (M = Cu, Ag); these compounds are isostructural, which enabled preparation of alloyed  $[(CH_3)_3SO]Cu_{2-x}Ag_xI_3$  compositions. The performed work provides a better understanding of the fundamental structure-property relationships in the Cu(I) and Ag(I) halide families. Moreover, a fabricated prototype X-ray detector based on  $[(CH_3)_3SO]M_2I_3$  demonstrated a very good detection sensitivity, indicating their potential for use in semiconductor X-ray detection applications.